Relative stability and magic numbers of nuclei deduced from behavior of cluster emission half-lives

M. Ismail,[1] W. M. Seif,[1,*] and A. Abdurrahman[2]
[1]*Department of Physics, Faculty of Science, Cairo University, Giza 12613, Egypt*
[2]*Department of Physics, Faculty of Engineering, Misr University for Science and Technology (MUST), Giza, Egypt*
(Received 25 May 2016; published 11 August 2016)

We calculated the half-life times (T_c) of the ^{14}C, ^{20}O, ^{20}Ne, and ^{24}Ne cluster emissions from heavy and superheavy nuclei. The variation of T_c with the neutron and proton numbers of daughter nuclei is studied to determine the minima in $\log_{10}T_c$ at each neutron number for different daughter isotones. We found that each minimum for a given isotone corresponds to neutron magicity already indicated by other approaches. The proton numbers at neutron magic numbers were found to be also proton magic numbers or differ slightly from them. We arranged the different isotones at each neutron magic number according to their stability in the sense that the more stable daughter isotone corresponds to the lowest value of $\log_{10}T_c$. The magic neutron numbers predicted by the present study are $N = 126$, 148, 152, 154, 160, 162, 172, 176, 178, 180, 182, 184, and 200. The predicted magic proton numbers are $Z = 82$, 98, 100 102, 106, 108, 114, and 116. The values of N and Z mentioned above agree with magic numbers deduced in other studies.

DOI: 10.1103/PhysRevC.94.024316

I. INTRODUCTION

The study of cluster radioactivity in heavy and superheavy nuclei (SHN) is one of the contemporary key topics in nuclear physics. Cluster radioactivity is the spontaneous emission of charged particles heavier than an α particle and lighter than fission fragments from an unstable nucleus. The phenomenon was first predicted on theoretical ground by Sandulescu *et al.* [1] in 1980. Experimentally, the phenomenon of cluster radioactivity as a new basic decay process was established by Rose and Jones [2] in 1984. They observed a spontaneous ^{14}C decay of ^{223}Ra with a half-life of 10^7 years. This prediction has been confirmed by Aleksandrov *et al.* [3], Gales *et al.* [4], and Price *et al.* [5] within the same year. After the pioneering work of Rose and Jones, the ^{14}C decay of other isotopes, such as ^{221,222,224,226}Ra, ^{223,225}Ac, ^{226}Th, and ^{221}Fr were detected [5–7]. Also, many other heavier cluster decays, such as ^{20}O, ^{24,26}Ne, ^{23}F, ^{28,30}Mg, and ^{32,34}Si from various heavy nuclei have been observed in several experiments [8–12]. The produced heavy nuclei in the observed decays of the cluster emitters from ^{221}Fr to ^{242}Cm are usually the doubly magic daughter $_{82}{}^{208}$Pb or one of its neighboring nuclei.

α decay has long been a useful tool for probing nuclear structure. It remains a very important experimental tool for providing information on ground-state properties, nuclear interaction, and stability of heavy and superheavy nuclei. For instance, the half-life time of the α emitters reflects the influences of the nuclear structure of the involved nuclei, such as their deformations [13], isospin asymmetry [14], the collective vibrational excitations [15], and the nuclear incompressibility [16]. Also, the α decay provides an important tool to investigate the cluster preformation probability inside parent nuclei [17–20] and the influences of the numbers of valence neutrons and protons, or holes, inside them [21] in addition to the corresponding ground-state spin parity, the nucleon shell closures [22–24], and the pairing effects [25–27]. However, we believe that cluster emissions can play the same role to investigate nuclear structure, such as α decays do.

Cluster radioactivity is closely connected with the intensive experimental activity on the synthesis and study of SHN in the past few decades [28,29]. One of the most popular approaches to study the spontaneous cluster emission is the preformed cluster model. The essential concept of this approach is that the cluster is considered to be preformed in the decaying nucleus with a certain preformation probability [30–34]. Clusters of different sizes would have different probabilities of being preformed inside the radioactive emitter. Hence, the formed light cluster could penetrate through the Coulomb barrier raised between it and the formed daughter with the decay Q value. Both the knocking frequency on the barrier and the penetration probability through it depend on the size of the emitted cluster and the Q value of the decay. The density-dependent cluster model [35] is one of the extended models based on this approach.

In the present paper, we aim to predict the proton and neutron magic numbers by investigating the nuclear stability for heavy and superheavy nuclei against cluster decays. We will do this by studying the variation of the half-life times of the cluster emitters against the number of protons and neutrons of the produced daughter nuclei. Towards our goal, we first summarize, in the next section, the method of calculating the half-life time in the framework of the density-dependent cluster model based on the M3Y-Reid nucleon-nucleon (NN) interaction. In Sec. III, we discuss the numerical details and results for the ^{14}C, ^{20}O, ^{20}Ne, and ^{24}Ne cluster emissions from the considered heavy and superheavy nuclei. The paper ends with a summary and conclusions presented in Sec. IV.

II. THEORETICAL FRAMEWORK

The effective potential between a preformed spherical cluster interacting with a deformed daughter nucleus inside

*wseif@sci.cu.edu.eg

a parent one can be written in the form

$$U_T(r,\beta) = \lambda_\beta\, U_N(r,\beta) + U_C(r,\beta) + U_\ell(r). \quad (1)$$

Here, $U_{N(C)}(r,\beta)$ defines the attractive nuclear (repulsive Coulomb) part of the interaction potential. The last term in Eq. (1) accounts for the additional centrifugal part of the potential, given in terms of orbital angular momentum (ℓ) carried by the emitted light cluster. β defines the emission angle. It represents the relative orientation angle of the symmetry axis of the participating deformed nucleus measured from the emitting vector joining the centers of mass of the two involved nuclei ($\vec{r}$) [36]. To guarantee a quasistationary state [37], the scaling factor λ_β is introduced to give the strength of the attractive part of the interaction potential [$U_N(r,\beta)$] at an emission angle β.

For a reliable cluster-daughter interaction potential, we will use the double-folding model based on the M3Y-Reid-Elliot potential with the zero-range exchange contribution,

$$v_N(r_{12}) = \left[7999\frac{\exp(-4r_{12})}{4r_{12}} - 2134\frac{\exp(-2.5r_{12})}{2.5r_{12}}\right] - 276\left[1 - 0.005\left(\frac{E_c}{A_c}\right)\right]\delta(r_{12}). \quad (2)$$

This potential was derived [38] by fitting to the elements of the G matrix of the Reid-Elliot nucleon-nucleon interaction. The energy of the emitted cluster is corrected for recoil $E_c = A_d Q/(A_c + A_d)$, where $A_c(A_d)$ is the mass number of the emitted cluster (daughter nucleus), Q is the Q value of the considered decay, and r_{12} is the separation distance between the two interacting nucleons.

In the framework of the double-folding model, the nuclear and Coulomb potentials are obtained as [39,40]

$$V_{N(C)}(\vec{r}) = \iint \rho_c(\vec{r}_1)v_{N(C)}(|r_{12}|)\rho_d(\vec{r}_2)d\vec{r}_1 d\vec{r}_2. \quad (3)$$

Here, $\vec{r}_1$ and $\vec{r}_2$ are the vectors describing the positions of the nucleons belonging to the emitted cluster (c) and the daughter nucleus (d), respectively, relative to their centers of mass [36]. $v_C(r_{12})$ is the standard proton-proton Coulomb force. The matter and charge-density distributions of the deformed nuclei are used in the two-parameter Fermi form [41] $\rho(r,\theta) = \rho_0/\{1 + \exp[r - R(\theta)]/a\}$. Here, θ is the angle between the position vector $\vec{r}$ and the symmetry axis of the nucleus. The orientation-dependent half-density radius (in femtometers) reads $R(\theta) = R_0[1 + \sum_{i=2\text{–}4,6}\beta_i Y_{i0}(\theta)]$. The radius and diffuseness parameters are fixed as $R_0 = 1.07\,A^{1/3}$ fm and $a = 0.54$ fm [35,42], respectively. $\beta_{i=2\text{–}4,6}$ are the multipole deformation parameters. For spherical nuclei, the half-density radius becomes constant $R = R_0$. For a given nucleus, the constant ρ_0 is obtained by normalizing the matter (charge-) density distribution to its mass number (atomic number). In the presence of deformed nuclei, the double-folding integrations are performed numerically using the multipole expansion method [36,43,44]. The centrifugal part of the potential in Eq. (1) will be considered in its Langer modified form $U_\ell(r) = (\ell + 1/2)^2\hbar^2/2\mu r^2$ [45]. This form, instead of the original one with $\ell(\ell + 1)$, is usually used to guarantee the correct behavior of the scattered radial wave function and the potential near the origin [46] with no significant change in the Coulomb barrier region of the potential. μ is the reduced mass of the cluster(m_c)-daughter(m_d) system $\mu = m_c m_D/(m_c + m_d)$.

The scaling factor λ_β of the nuclear potential part [Eq. (1)] is determined separately for each emission angle β [47] using the Bohr-Sommerfeld quantization condition [48],

$$\int_{R_1(\beta)}^{R_2(\beta)} k(r,\beta)dr = (2n+1)\frac{\pi}{2}. \quad (4)$$

$k(r,\beta) = \sqrt{2\mu|U_T(r,\beta) - Q|/\hbar^2}$ is the wave number. $R_{1,2}(\beta)$ and $R_3(\beta)$, that will be mentioned below, represent three classical turning points given as $U_T(r,\beta)|_{r=R_i(\beta)} = Q_c$. They define the relevant internal pocket and Coulomb barrier regions of the total interaction potential. The condition given by Eq. (4) ensures an integer number of nodes for the quasibound radial wave function of the cluster-daughter system [46]. For the nuclear interaction potentials characterized with no repulsive core, such as that based on the M3Y-type of NN force, we can use the Wildermuth quantization condition to relate the quantum number n to the shell model [49–51] $2n = G - \ell$. The global quantum number (G) is given in terms of the oscillator quantum numbers of the nucleons belonging to the cluster inside the parent nucleus ($g_i^{(A_d+A_c)}$), and the internal quantum numbers of them given in the individual emitted cluster ($g_i^{(A_c)}$) as [50]

$$G = 2n + \ell = \sum_{i=1}^{A_c}\left(g_i^{(A_d+A_c)} - g_i^{(A_c)}\right). \quad (5)$$

The values of $g_i(50 \leqslant Z,N \leqslant 82) = 4$, $g_i(82 < Z,N \leqslant 126) = 5$, $g_i(126 < N \leqslant 184) = 6$, and $g_i(N > 184) = 7$ are considered. These values correspond to the $4\hbar\omega$, $5\hbar\omega$, $6\hbar\omega$, and $7\hbar\omega$ harmonic-oscillator shells, respectively.

The half-life time ($T_{1/2}$) of a given parent nucleus against a specific cluster decay can be obtained in terms of the decay width (Γ_c) and the cluster preformation probability (S_c) as

$$T_{1/2} = \frac{\hbar\ \ln 2}{S_c\Gamma_c}. \quad (6)$$

The decay width is defined as $\Gamma_c = \hbar\nu_c P_c$. Here, ν_c and P_c are the tunneling knocking frequency and the quantum penetration probability of the emitted cluster, respectively. As a cold spontaneous process, the decay width of the cluster decay can be considered along the noncompact optimum orientation of the deformed nucleus. It is shown that, in order to account for nuclear deformation properly, it is more relevant to obtain the cluster decay width by averaging over all possible orientations of the involved deformed nuclei, rather than considering the noncompact optimum orientation [52]. The orientation-averaged decay width is obtained as

$$\Gamma_c = \frac{\hbar}{2}\int_0^\pi \nu_c(\beta)P_c(\beta)\sin\ \beta\ d\beta. \quad (7)$$

At a certain emission angle β, the cluster knocking frequency and the penetration probability based on the Wentzel-Kramers-Brillouin (WKB) tunneling approximation are given,

respectively, by

$$\nu_c(\beta) = T^{-1}(\beta) = \left[\int_{R_1(\beta)}^{R_2(\beta)} \frac{2\mu}{\hbar k(r,\beta)} dr\right]^{-1}, \quad (8)$$

and

$$P_c(\beta) = \exp\left(-2\int_{R_2(\beta)}^{R_3(\beta)} k(r,\beta) dr\right). \quad (9)$$

T represents the time required to traverse the internal potential pocket between the first two turning points, back and forth [46,53].

For the cluster decays of known half-lives ($T_{1/2}^{\text{expt.}}$) and using the calculated decay width, we can estimate the preformation probability of the emitted cluster inside the corresponding parent nucleus from Eq. (6),

$$S_c = \frac{\hbar \ln 2}{\Gamma_c \, T_{1/2}^{\text{expt}}}. \quad (10)$$

The transferred angular momentum (ℓ) conserves the spin and parity in the decay process. When the emitted cluster is an even(Z)-even(N) nucleus having ground-state spin(J)-parity(π) $J_c^{\pi} = 0^+$, the conditions satisfying the conservation laws of spin and parity become $|J_p - J_d| \leqslant \ell \leqslant |J_p + J_d|$ and $\pi_p = \pi_d(-1)^{\ell}$. p and d define the parent and daughter nuclei, respectively. Following the principle of least action, we consider the minimum value of ℓ satisfying the two mentioned conditions. The spin-parity assignments for the ground states of the involved nuclei are taken from Ref. [12]. ℓ is considered zero whenever the spin and parity of any of the participating nuclei are not measured.

III. RESULTS AND DISCUSSION

The aim of the present paper is to predict the neutron and proton numbers in heavy and superheavy nuclei at which a nucleus is more stable compared to the neighboring nuclei. This is performed by studying the behavior of $\log_{10}T_c$ of four different cluster (^{14}C, ^{20}O, ^{20}Ne, and ^{24}Ne) emissions with the variation of neutron and proton numbers of the daughter nucleus. We consider even(Z)-even(N) and odd-A elements with Z values in the range of $85 \leqslant Z \leqslant 122$. For this purpose we investigated a total number of 7436 cluster decay processes in this paper. The Q values of the mentioned decays are obtained from the mass excess of the involved nuclei [54]. Atomic masses missed in Ref. [54] are taken from the theoretical calculations of masses in Ref. [55].

As mentioned above, one of the fundamental quantities required for the calculations of the half-lives is the cluster preformation probability (S_c). The exponential formula,

$$S_c = 10^{-a\sqrt{\mu Z_c Z_D}+b} \quad (11)$$

TABLE I. The cluster preformation probabilities $S_c^{\text{expt.}}$ (last column) estimated using Eq. (10) from the measured half-lives $T_{1/2}^{\text{expt.}}$(s) [12] (column 3) and the calculated decay widths (column 7) for the cluster emitters listed in column 1. The emitted clusters and the corresponding Q values [54] are presented in columns 2 and 4, respectively. The decay widths are calculated in terms of the WKB penetration probability and knocking frequency with an interaction potential based on the M3Y-Reid NN interaction. The global quantum numbers G [Eq. (5)], which are used to find the quantum numbers n in the Bohr-Sommerfeld condition [Eq. (4)], and transferred angular momenta (ℓ) by the outgoing clusters are listed in columns 5 and 6, respectively.

Parent	Cluster	$\log_{10}[T_{1/2}^{\text{expt.}}(\text{s})]$	Q (MeV)	G	ℓ	$\log_{10}[\Gamma_c(\text{MeV})]$	$S_c^{\text{expt.}}$ [Eq. (10)]
^{221}Fr	^{14}C	14.51	31.29	67	3	− 8.07	5.00×10^{-5}
^{221}Ra	^{14}C	13.37	32.40	67	3	− 6.94	5.10×10^{-5}
^{222}Ra	^{14}C	11.05	33.05	68	0	− 5.42	3.24×10^{-4}
^{223}Ra	^{14}C	15.05	31.83	68	4	− 7.94	1.05×10^{-5}
^{224}Ra	^{14}C	15.90	30.54	68	0	− 10.25	3.09×10^{-4}
^{226}Ra	^{14}C	21.29	28.20	68	0	− 15.37	1.66×10^{-4}
^{225}Ac	^{14}C	19.28	30.48	68	4	− 11.61	2.94×10^{-6}
^{228}Th	^{20}O	20.73	44.72	92	0	− 14.07	2.98×10^{-5}
^{231}Pa	^{23}F	26.02	51.86	103	1	− 15.85	9.16×10^{-9}
^{230}U	^{22}Ne	19.56	61.39	98	0	− 12.63	1.61×10^{-5}
^{230}Th	^{24}Ne	24.61	57.76	104	0	− 16.42	8.80×10^{-7}
^{231}Pa	^{24}Ne	22.89	60.41	105	1	− 13.57	6.55×10^{-8}
^{232}U	^{24}Ne	20.39	62.31	106	0	− 11.96	5.08×10^{-7}
^{233}U	^{24}Ne	24.84	60.49	106	2	− 14.70	9.80×10^{-9}
^{234}U	^{24}Ne	25.93	58.83	106	0	− 17.23	2.73×10^{-7}
^{235}U	^{25}Ne	27.44	57.71	110	3	− 19.57	1.84×10^{-6}
^{234}U	^{26}Ne	25.93	59.42	114	0	− 17.08	1.93×10^{-7}
^{234}U	^{28}Mg	25.74	74.11	118	0	− 16.06	2.89×10^{-8}
^{235}U	^{28}Mg	27.44	72.43	118	1	− 18.43	1.34×10^{-7}
^{236}Pu	^{28}Mg	21.65	79.67	120	0	− 11.39	7.52×10^{-9}
^{238}Pu	^{28}Mg	25.66	75.91	120	0	− 16.33	6.40×10^{-8}
^{238}Pu	^{30}Mg	25.66	76.80	128	0	− 15.60	1.19×10^{-8}
^{238}Pu	^{32}Si	25.30	91.19	132	0	− 15.31	1.41×10^{-8}
^{242}Cm	^{34}Si	23.11	96.51	142	0	− 12.01	1.09×10^{-9}

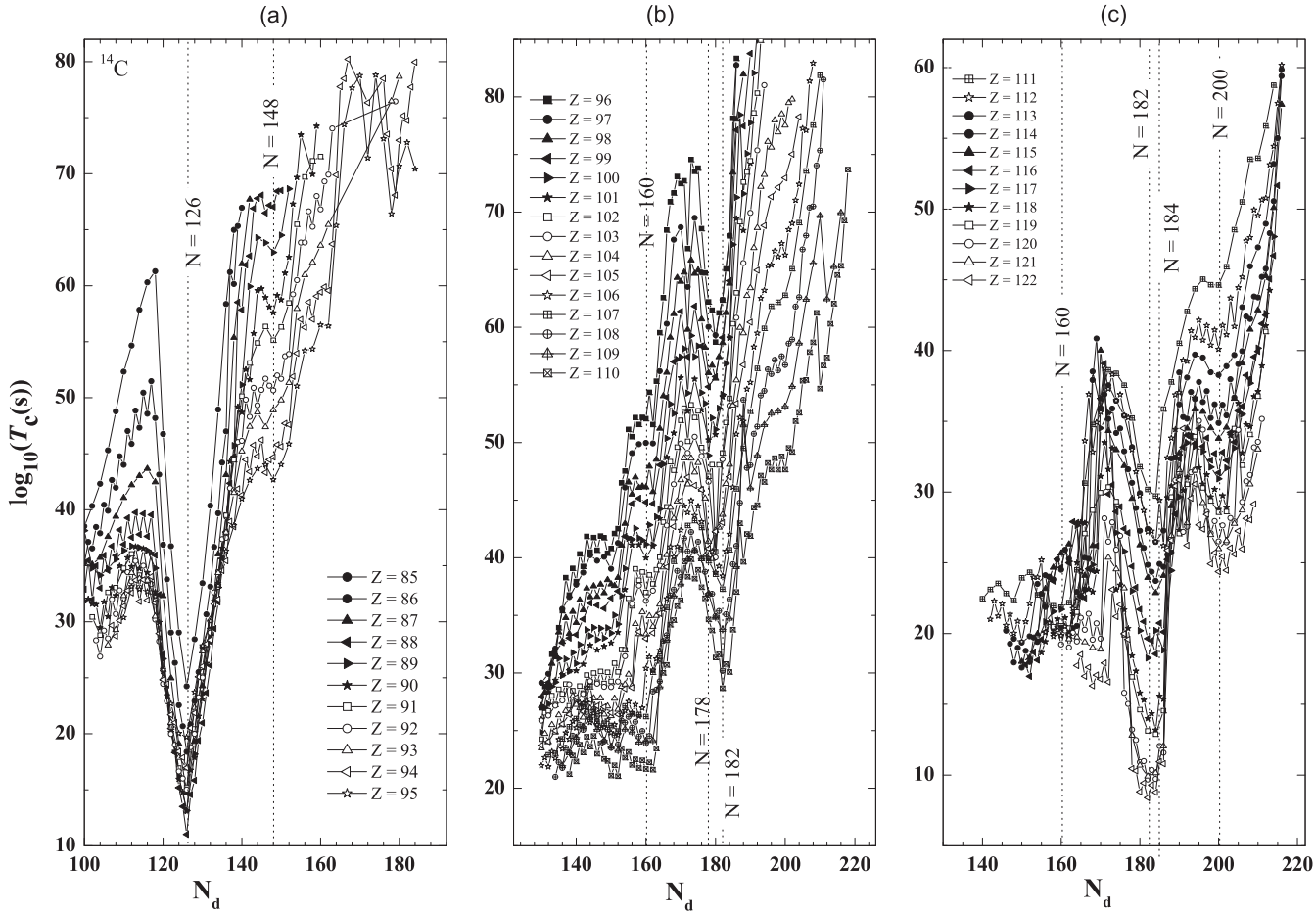

FIG. 1. The decimal logarithm of the half-lives of heavy and superheavy nuclei (Z_p = 85–122) against ^{14}C cluster decay versus the neutron number of the daughter nucleus. Calculations are performed within the density-dependent cluster model based on the M3Y-Reid NN interaction as discussed in the text. The vertical dotted lines correspond to the indicated possible neutron magic numbers.

has been suggested in Ref. [56] to give the cluster preformation probability. Here, $\mu = A_c A_d/(A_c + A_d)$ is the reduced mass in nucleon mass units. $Z_c(Z_d)$ is the atomic number of the emitted cluster (daughter nucleus). We will determine the values of the free parameters a and b using the available experimental half-lives ($T_{1/2}^{\text{expt.}}$) Eq. (10). Shown in Table I are the values of the cluster preformation probability $S_c^{\text{expt.}}$ as deduced using Eq. (10) from the experimental half-lives $T_{1/2}^{\text{expt.}}$(s) [12] and the calculated decay widths [Eqs. (7)–(9)] for the presented cluster emitters, which have known $T_{1/2}^{\text{expt.}}$. We used the obtained $S_c^{\text{expt.}}$ for the cluster decays mentioned in Table I to find the a and b parameters of the formula given by Eq. (11). Upon fitting to the obtained results of the even-even (e-e) and odd-A cluster emitters, Table I, we found that the preformation factor can be reproduced by Eq. (11) with the values $a = -0.052\,32$, $b_{\text{e-e}} = 0.746\,75$ and $b_{\text{odd}-A} = -0.29\,701$. Now, we can employ this parametrization of the preformation probability to perform precise calculations of cluster emission half-lives.

Figure 1 shows the variation of $\log_{10}T_c$ for the ^{14}C cluster emissions from parent nuclei with atomic numbers in the range of $85 \leqslant Z_p \leqslant 122$ as a function of the neutron number of the daughter nucleus. This figure shows clearly a deep minimum in the calculated half-lives of the ^{14}C cluster emission at daughter neutron number $N_d = 126$, for all mentioned Z_p values. The deepest minimum is for the parent nucleus with atomic number $Z_p = 88$. This is a fingerprint for formation of the double magic nucleus ^{208}Pb. However, $\log_{10}T_c$ for a given group of isotopes becomes a minimum for the isotope with the daughter nucleus having larger stability. For different elements the arrangement of the points at minima can be taken as a measure of stability of the resulting daughter nuclei. Although the upper point corresponds to less stability, the lowest one has the highest one.

In Table II, the heavy and superheavy nuclei are arranged in order of indicated decreasing stability of the daughter nuclei by the present calculations. Table II presents the neutron numbers of daughter nuclei at which minima in $\log_{10}T_c$ are obtained for the four cluster emission processes (^{14}C, ^{20}O, ^{20}Ne, and ^{24}Ne) studied systematically in the present paper. For each neutron number we arranged the atomic numbers of daughter nuclei (Z_d) in order of decreasing stability (increasing values of $\log_{10}T_c$). Table II shows that the obtained neutron numbers at minima are neutron magic numbers almost indicated in other studies [57–73]. Some of these studies are based on minimizing

TABLE II. Heavy and superheavy nuclei arranged in order of decreasing stability and neutron magic numbers predicted in the present paper. The proton and neutron magic numbers that appeared in previous studies and confirmed in this paper are italicized and bolded. Neutron magic numbers resulting from the present calculations are underlined.

Cluster	N_d	Z_d (daughter)
^{14}C	***126***	***82***, 83, 84, 81, 86, 85, 87, 88, 80, 90, 89, 94, 96, 92, 97, 95, 91, 93, and 79
	148	89, 86, 85, 84, and 83
	160	107, ***106***, 105, ***102***, 99, 97, 96, and 95
	178	99, 94, 95, 93, and 89
	182	***116***, 115, and 111 and 104, ***102***, 103, 101, and ***100***
	184	***114***, 113, 112, 110, 109, ***108***, 107, and 105
	200	***116***, 115, ***114***, 113, 112, 111, 110, 109, ***108***, 107, ***106***, 105, and ***100***
^{20}O	***126***	***82***, 81, 83, 84, 80, 85, 86, 79, 87, 88, 78, 89, and 77
	154	104, ***102***, 101, ***98***, and 99
	162	***108***, 109, 112, and 107
	178	***102***, ***100***, 101, 99, ***98***, and 97
	180	87, 86, 85, 84, 83, and ***82***
	182	***114***, 113, 112, 111, 110, 109, ***108***, 107, 104, and 105
	200	***108***, ***106***, 105, and 104
^{20}Ne	***126***	***82***, 78, 77, 76, and 75
	180	112, 111, 110, and 109, and 103, ***102***, ***100***, and ***98***
^{24}Ne	***126***	***82***, 81, 83, 84, 80, 86, 85, 88, 87, 79, 94, 90, 89, 92, 78, 95, 91, 93, 77, 76, and 75
	152	***102***, ***100***, 103, 101, 99, ***98***, 97, and 96
	172	95, 94, 90, 91, 89, 88, 87, and 86
	176	***100***, ***98***, 97, and 96
	180	112, 111, 110, 109, ***108***, 107, ***106***, 105, ***102***, and 103
	200	112, 111, 110, 109, and ***108***

the total energy of the nucleus after including both shell and residual pairing correction energies and others based on self-consistent calculations of the nuclear energy levels. At each neutron number, the daughters' atomic numbers producing minima are magic proton numbers or near these numbers. The proton and neutron magic numbers appeared in previous studies and confirmed in the present paper are italicized and bolded. We underlined the neutron magic numbers resulting from the present calculations.

As presented in Table II, above the lowest point of the daughter isotopes having $Z_p = 82$, there are 18 lowest points whose Z_d values are arranged in order of increasing $\log_{10}T_c$. The daughter nuclei associated with these lowest points having neutron numbers of $N = 126$. As shown in Fig. 1(a), ten of these lowest points lie above the lowest point of the $Z_d = 88$ curve. Let us consider the parent nuclei of $Z_p = 89$, 90, 87, 92, 91, 93, and 94. It is known that the upper level in the proton closed shell $Z = 82$ is the $3s_{1/2}$ level [57]. Above this closed shell is the level $1h_{9/2}$. The arrangement of points with different Z_p values at the minima shows decreasing stability for the daughter nuclei with Z_d values 83, 84, 81, 86, 85, 87, and 88, respectively. The emitted six protons in the ^{14}C cluster for the parent nuclei with $Z_p = 88$, 89, 90, and 91 comes from the $h_{9/2}$ level which can be filled by ten protons. After emission of the cluster, the number of protons in the $h_{9/2}$ level becomes zero through three protons, respectively. For the parent nucleus with $Z_p = 94$, the protons above the closed shell are arranged as ten protons in $h_{9/2}$ and two protons in the above level $2f_{7/2}$, and this means that the protons of the ^{14}C cluster come from two different levels. This is the case also for the parent $Z_p = 87$ where the protons come from the $h_{9/2}$ and $3s_{1/2}$ levels. The upper point in the minima in Table II is for $Z_p = 85$ ($Z_d = 79$). For $Z_p = 85$, a proton in the level below $3s_{1/2}$ should contribute to the emission process. This means that emission of the cluster protons comes from three energy levels. It is clear that the nuclei with $Z_p = 85$ do not prefer ^{14}C cluster emission whereas the nucleus $Z_p = 88$ prefers ^{14}C emission leaving the double magic nucleus ^{208}Pb.

Also in Fig. 1(a), a minimum appear at $N_d = 148$ for each of the parent nuclei with $Z_p = 95, 92, 91, 90$, and 89, arranged in order of increasing $\log_{10}T_c$. These minima are not as deep as those at $N_d = 126$. This means that the isotones with $N_d = 148$ have decreasing stability for the elements with $Z_d = 89$, 86, 85, 84, and 83, in the sense that ^{231}Bi is less stable between these elements. It should be noted that $N = 148$ is considered as a neutron magic number [58]. Minimization of the total energy of nuclei calculated by Skyrme force and after the addition of the shell effect produces a minimum at the neutron number $N = 148$ [58].

Minima are shown also in Fig. 1(b) at $N_d = 160$ corresponding to $Z_d = 99$, 97, 96, and 95. As Z increases, minima appear again in Fig. 1(c) at the same neutron number corresponding to $Z_d = 107$, 106, 105, and 102. The values of the daughters' proton numbers are arranged in order of decreasing stability. $N = 160$ is considered as a neutron magic number in Refs. [59,60]. A clear minimum exists also in Fig. 1(b) at $N_d = 178$ for each of the parent nuclei with $Z_p = 105$, 100, 101, 99, and 95, in order of increasing

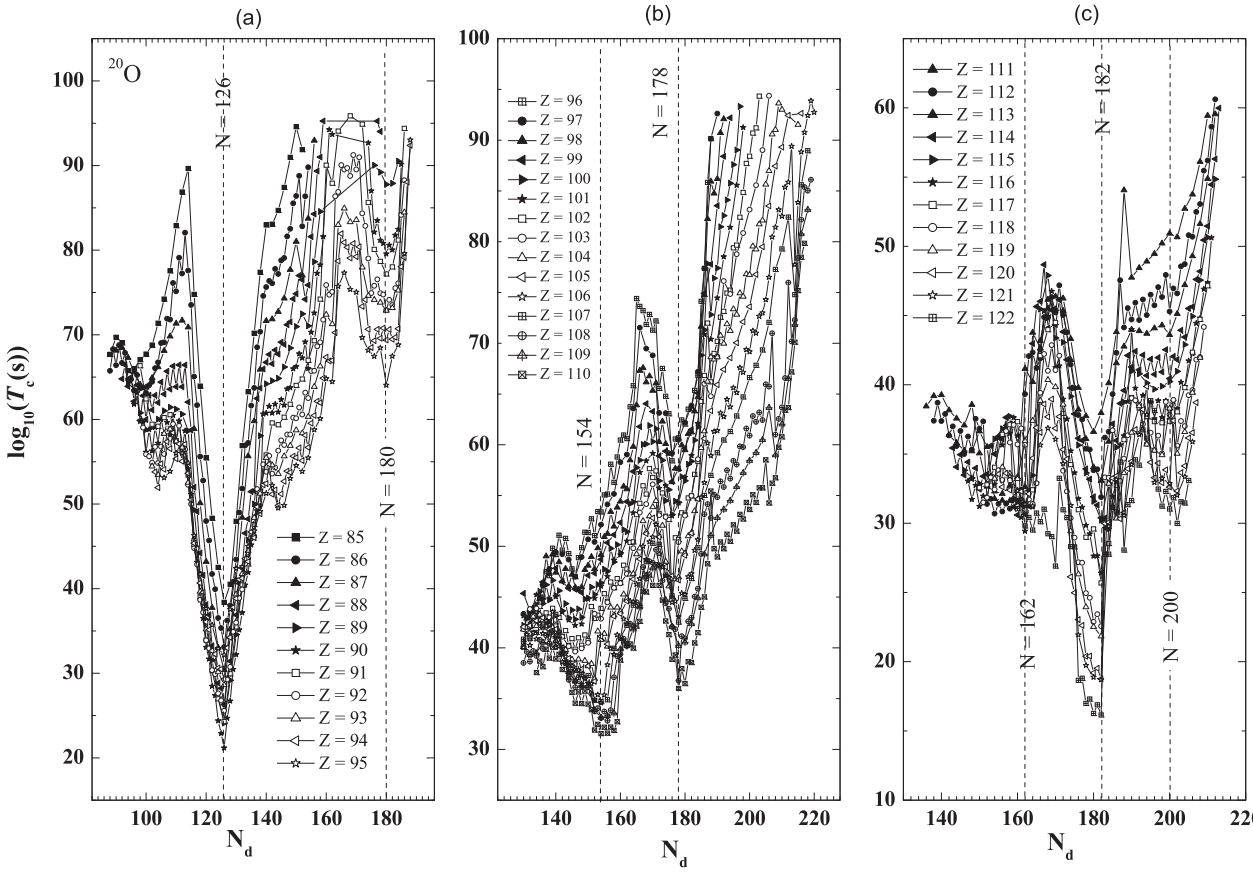

FIG. 2. The same as Fig. 1 but for ^{20}O cluster decays.

$\log_{10}T_c$. Thus the isotones with $N_d = 178$ can be arranged in order of decreasing stability as $Z_d = 99$, 94, 95, 93, and 89. In Ref. [58], the neutron number $N = 178$ is expected as a neutron magic number. Other clear minima appear at $N_d = 182$ in Fig. 1(b) at which the points are arranged in the order of decreasing stability as $Z_d = 104$, 102, 103, 101, and 100, respectively, and then with $Z_d = 116$,115,111 in Fig. 1(c).

On the other hand, Fig. 1(c) shows that the curves for Z_p values 120, 119, 118, 116, 115, 114, 113, and 111, arranged in order of increasing $\log_{10}T_c$, tend to produce shallow minima at $N_d = 184$. The isotones at this neutron number have stability decreasing in the order $Z_d = 114$, 113, 112, 110, 109, 108, 107, and 105. It should be noted that $N = 184$ is found to be a semimagic neutron number in Refs. [58,61,62,63]. $Z = 114$ is indicated as a proton magic number in Ref. [58]. Moreover, too shallow minima exist in Fig. 1(c) at $N_d = 200$ for the elements with $Z_d = 111$, 110, 109, 108, 107, 106, and 105. At the same neutron number of the daughter nucleus ($N_d = 200$), shallow minima occur for higher values of Z_p in the range of $118 \leqslant Z_p \leqslant 122$. $Z = 116$ is found to be a proton deformed magic number in Refs, [64,65]. For these Z_p values, sudden increases in $\log_{10}T_c$ appear after $N_d = 186$. For $N_d = 178$, 180, 182, 184, and 186, the values of $\log_{10}T_c$ for $Z_p = 122$, 121, and 120, which correspond to the daughter nuclei with $Z_d = 116$, 115, and 114, respectively, are almost the same. This means similar stability for elements in these N and Z ranges. However, from the behavior of $\log_{10}T_c$ of the ^{14}C cluster emission with proton and neutron numbers, we find that $\log_{10}T_c$ has a minimum value when the proton or neutron numbers of the corresponding daughter nucleus are magic numbers. The indicated values of magic numbers in our analysis agree with the numbers deduced by other authors based on different methods [58–65]. For each neutron magic number, we arranged different isotones according to their stability, Table II. We found that one of the Z_d values for these different isotones is a magic number or near a magic number.

Figure 2 shows the variation of $\log_{10}T_c$ for parent nuclei with atomic numbers in the range of $85 \leqslant Z_p \leqslant 122$ against ^{20}O cluster emissions as a function of N_d. As shown in Fig. 2(a), the neutron magic number $N_d = 126$ appears clearly at all presented Z_p values. The elements with $Z_d = 82$, 81, 83, 84, 80, 85, 86, 79, 87, 88, 78, 89, and 77 are arranged in Table II in order of decreasing nuclear stability. The less stable isotone is $Z_d = 77$, which loses three protons from the level below the top of magic number $Z = 82$. For the nuclei $80 \leqslant Z_d \leqslant 86$, the corresponding values of $\log_{10}T_c$ are less than 30. This shows the relative stability of nuclei near the doubly magic nucleus ^{208}Pb. Clear minima also exist in Fig. 2(a) at $N_d = 180$ for the isotopic chains of the elements $Z_p = 95$, 94, 93, 92, 91, and 90 (in order of increasing $\log_{10}T_c$) with respective correspondence to the daughters $Z_d = 87$, 86, 85, 84, 83, and 82. These nuclei have high-(N/Z) ratios, and so the masses of which are calculated theoretically. They cannot be synthesized easily in the near future.

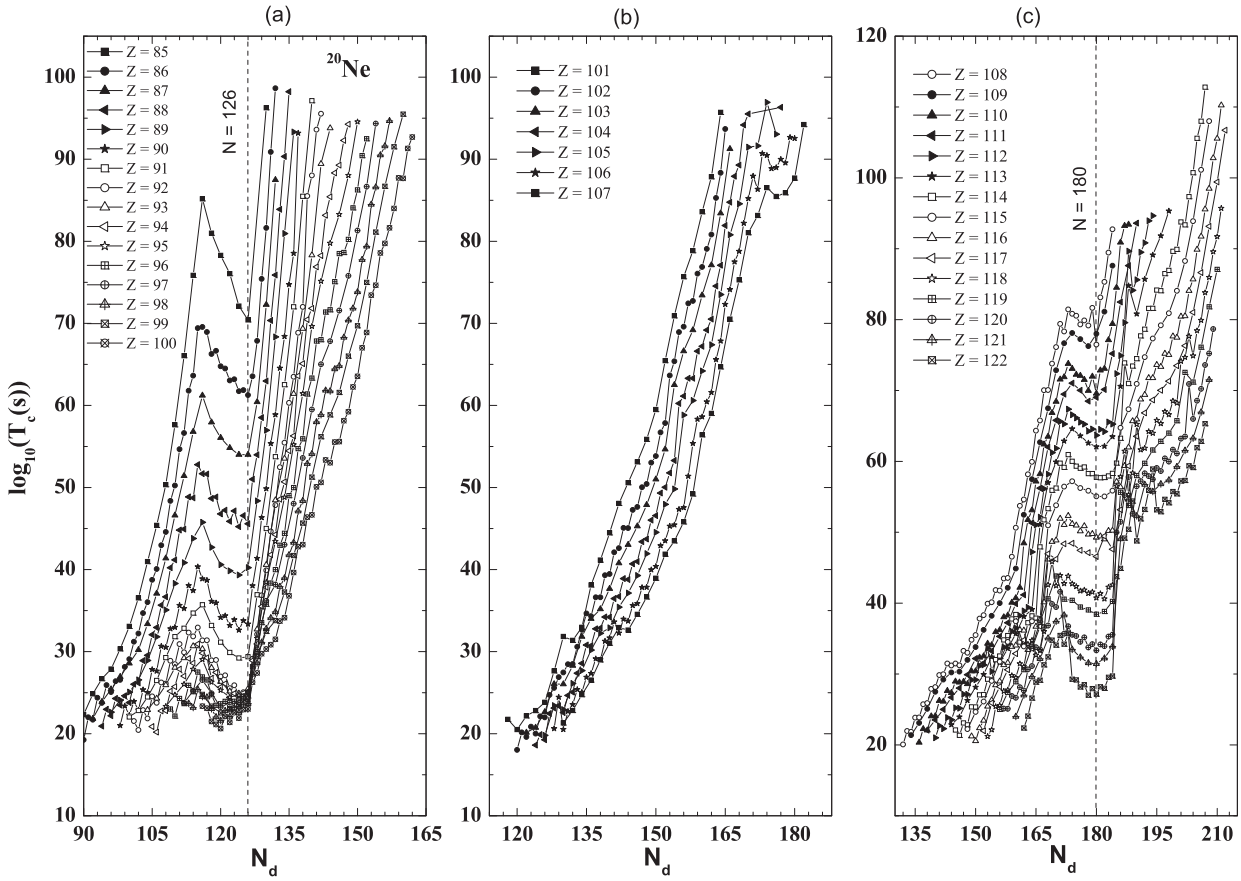

FIG. 3. The same as Fig. 1 but for ^{20}Ne cluster decays.

In Fig. 2(b), some minima exist at $N_d = 154$ for the elements corresponding to $Z_d = 104$, 102, 101, 98, and 99. Minima of $\log_{10}T_c$ curves appear corresponding to daughter isotones of $N_d = 162$ in Fig. 2(c). These isotones are arranged in decreasing order of their stability as $Z_d = 108$, 109, 112, and 107. Although $N = 162$ was found to be a neutron magic number in Refs. [61–64,66], $Z = 108$ was assigned as a proton magic number in Refs. [61,64,65,67,68,69]. As Z_d increases, minima appear at $N_d = 178$ in Fig. 2(b) for Z_d values in the range of $97 \leqslant Z_d \leqslant 102$. The lowest two minimum points at this neutron number are for $Z_d = 102$ and 100. Whereas $N_d = 178$ was deduced as a neutron magic number in Refs. [58,69], $Z = 102$ was assigned to be a proton magic number in Refs. [19,67], and the nucleus with $Z = 102$ and $N = 178$ is indicated as a doubly magic nucleus. The highest two points among the minimal points corresponding to $N_d = 178$ are for the two isotones of $Z_d = 98$ and 97. By increasing the values of Z_d, clear minima appear in Fig. 2(c) at $N_d = 182$ for $Z_d = 114$, 113, 112, 111, 110, 109, 108, 107, 104, and 105, respectively. Moreover, our calculations indicate the stability of the daughter nucleus ^{292}108, which has $N_d = 184$. Figure 2(c) shows also that after $N_d = 182$ a sudden increase in $\log_{10}T_c$ appears for Z_d values in the range of $110 \leqslant Z_d \leqslant 114$. The lowest points in this case are those of $Z_d = 114$, 113, 112, 111, and 110 as arranged in order of increasing $\log_{10}T_c$. Eventually, few weak minima appear in Fig. 2(c) at $N_d = 200$. These points correspond to the daughter nuclei of $Z_d = 108$, 106, 105, and 104 in order of decreasing stability. $Z = 106$ is indicated as a proton magic number in Refs. [60,68,70].

Figure 3 shows the behavior of $\log_{10}T_c$ for the possible ^{20}Ne cluster emitters of different atomic numbers with increasing the neutron numbers of the produced daughter nucleus. As seen in Fig. 3(a), clear minima are obtained at $N_d = 126$, which is a neutron magic number. The points at these minima are arranged in order of increasing $\log_{10}T_c$ (decreasing stability of the daughter nuclei) as $Z_d = 82$, 78, 77, 76, and 75. As expected, the most stable nucleus having $N_d = 126$ is ^{208}Pb, which has double magic numbers for protons and neutrons. Shown in Fig. 3(c) are several deep minima appearing at $N_d = 180$. These minima correspond to daughter nuclei with $Z_d = 103$, 102, 100, and 98 and then with $Z_d = 112$, 111, 110, and 109 as arranged in order of decreasing stability. In the range of $105 \leqslant Z_d \leqslant 111$, $\log_{10}T_c$ becomes almost constant in the neutron variation range of $174 \leqslant N_d \leqslant 184$. For the daughter nuclei with neutron numbers larger than $N_d > 184$, a sudden increase in $\log_{10}T_c$ occurs for all values of Z_d. This indicates the important role of the shell effects in the behavior of the half-life time.

Presented in Fig. 4 is the variation of $\log_{10}T_c$ for parent nuclei of different atomic numbers in the range of $85 \leqslant Z_p \leqslant 122$ against ^{24}Ne cluster emissions as a function of N_d.

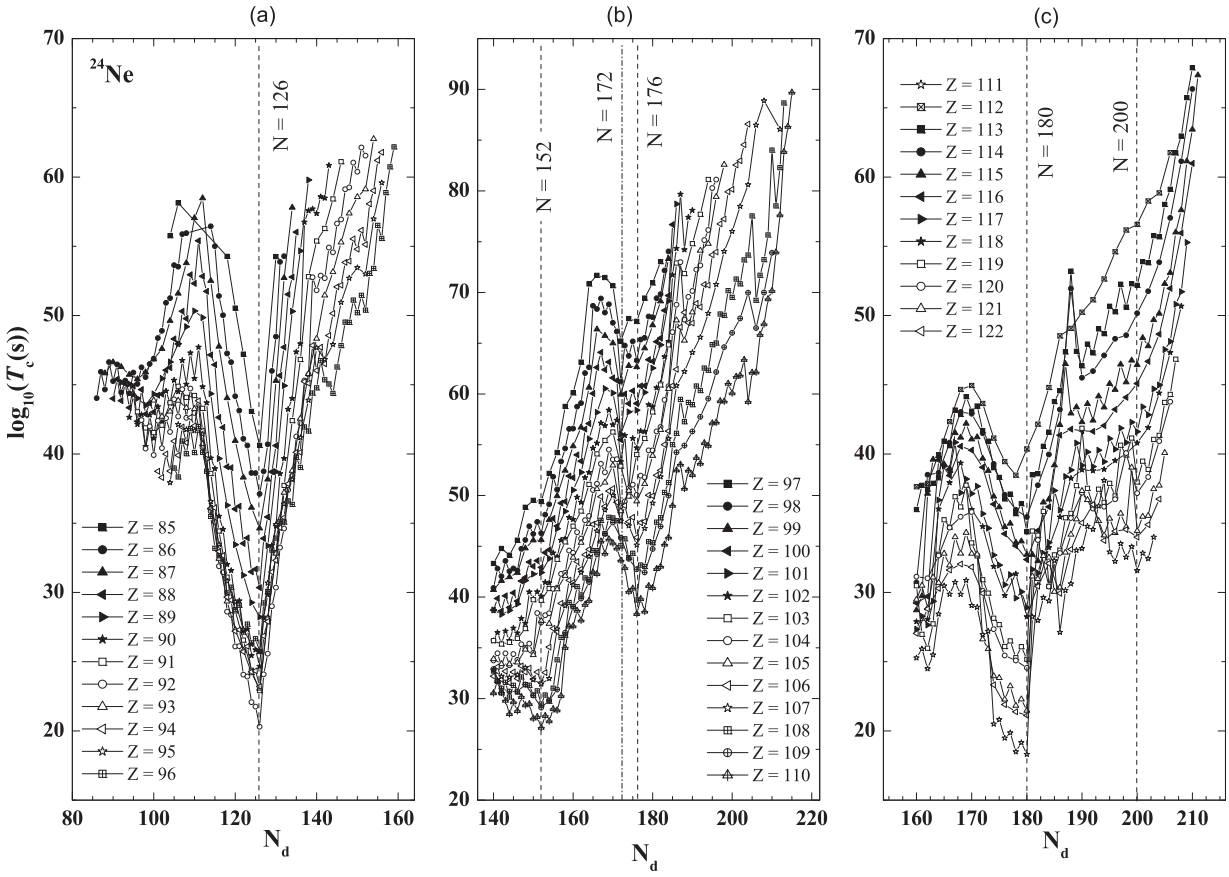

FIG. 4. The same as Fig. 1 but for ^{26}Ne cluster decays.

Regarding the neutron magic number $N_d = 126$, the deep minima at different Z_d values in Fig. 4(a) are similar to those found in Fig. 3(a). Figure 4(b) shows clear minima at $N_d = 152$ for daughter nuclei with $Z_d = 102$, 100, 103, 101, 99, 98, 97, and 96. $N = 152$ is found to be a neutron magic number in Refs. [62,66–69] and other studies. $Z = 102$ was indicated as a proton magic number in Refs. [19,67]. The nucleus with $Z = 100$ and $N = 152$ is predicted as a double magic nucleus in Refs. [64,71]. $Z = 98$ is indicated as a possible semimagic number of protons in Ref. [72]. Moreover, in Fig. 4(b) minima appear for the first time in the present paper at $N_d = 172$. These minima correspond to the daughters having $Z_d = 95$, 94, 90, 91, 89, 88, 87, and 86, respectively, where the daughters are arranged in decreasing order of stability. $N = 172$ is found to be a possible neutron magic number in Refs. [62,63,73]. Other minima are obtained in Fig. 4(b) at $N_d = 176$ corresponding to the daughters 100, 98, 97, and 96. As the neutron number increases, minima are found in Fig. 4(c) at $N_d = 180$ for $Z_d = 112$, 111, 110, 109, 108, 107, 106, 105, 102, and 103. We mentioned above that the proton numbers 102, 106, and 108 were indicated to be magic or semimagic numbers in different studies based on different treatments. Minima corresponding to $N_d = 200$ appear for the third time in this paper in Fig. 4(c) for the parent nuclei of $Z_p = 122$, 121, 120, 119, and 118 corresponding to $Z_d = 112$, 111, 110, 109, and 108, respectively.

In the present study of the variation of cluster emission half-life time with neutron numbers, we assumed that the outgoing clusters have spherical shapes. Cluster deformations reduce the calculated half-life time by a value that depends on the values of the deformation parameters and the volumes of the interacting nuclei [47]. This reduction is expected to be small for cluster volumes much smaller than the volumes of the corresponding daughter nuclei. In our orientation-averaged calculations, the logarithm of the half-life time ($\log_{10}T_c$) of ^{228}U against its ^{20}Ne decay decreases upon adding the deformation of ^{20}Ne by the value of -0.44. For the ^{20}O decay of ^{228}Th, the value of $\log_{10}T_c$ decreases after considering the ^{20}O deformation by the value of -0.01. The calculated $\log_{10}T_c$ of ^{230}Th, ^{231}Pa, ^{232}U, ^{233}U, and ^{234}U against their ^{24}Ne decay decreases upon considering the deformation of ^{24}Ne by the values of -0.62, -0.61, -0.73, -0.62, and -0.63, respectively. As we see, including the deformations of light-emitted clusters reduces the calculated half-life time by less than one order of magnitude. However, considering cluster deformations besides deformations of the daughter nuclei makes the calculations too difficult, but we can say that it does not affect our conclusions. In general, cluster deformations will not affect the behavior of the curves in our figures since each figure is for only one cluster and the reduction of the half-life time will be almost the same for all daughter nuclei in the figure. On the other hand, the neutron density distributions of heavy nuclei generally have larger

root-mean-square radii and are more diffuse than the corresponding proton distributions [74]. The difference between the two density distributions forms the so-called "neutron skin," which is related to the nuclear symmetry energy. Like the results obtained for α decays [75], the neutron skin thickness is expected to yield shorter half-life times and smaller preformation probability.

The above discussion shows that the theoretical calculation of the half-life time of different cluster emissions can produce neutron and proton magic numbers of heavy and superheavy nuclei. Moreover, it indicates the relative stability of nuclei neighboring proton or neutron magic numbers. It should be noted that the experimental half-life times of cluster emissions, heavier than the α particle, are not measured except for a few numbers of nuclei. The only quantity derived from experiment and used in calculating $\log_{10}T_c$ is the Q value for each decay. We found that the behavior of the calculated $\log_{10}T_c$ with a variation of N and Z of the considered nuclei produces almost the proton and neutron magic and semimagic numbers deduced from other different methods, such as minimization of the total energy [58] and the Hartree-Fock calculations. This means that the theory used in treating cluster emission and the Q value contains correct information on the properties of the heavy and superheavy nuclei. We recall here that the NN interaction used in minimizing the total energy in Ref. [58] is the well-known Skyrme-type interaction whereas the cluster emission model used here is derived from the M3Y-Reid NN force. The two NN forces differ in many aspects. For example, the first produces correctly the binding energy of several nuclei whereas the second fails to give nuclear structure properties. Finally, our present calculations show that the half-life times of the cluster emissions contain information about the internal structure of parent and daughter nuclei, such as the α emissions do [27,57,76,77].

IV. SUMMARY AND CONCLUSIONS

In the framework of the deformed density-dependent cluster model we calculated the half-life times of cluster emissions (T_c) for the four different clusters ^{14}C, ^{20}O, ^{20}Ne, and ^{24}Ne. We considered 7436 cluster decay processes and studied, for each cluster emission, the variation of $\log_{10}T_c$ with the proton and neutron numbers of the emitted daughter nuclei. For each cluster emission, we represented the neutron number variation of $\log_{10}T_c$ for different elements with atomic numbers in the range of $85 \leqslant Z \leqslant 122$. We found that the variations of $\log_{10}T_c$ with the number of neutrons in daughter nucleus (N_d) for different elements have minima at specific values of N_d. The first group of minima in the considered Z range occurs at $N_d = 126$, which is well-known neutron magic number. The deepest minimum at this N_d value corresponds to the double magic nucleus ^{208}Pb, which has extremely large stability. At this N_d value, the different isotones were arranged in order of decreasing stability according to their value of $\log_{10}T_c$. The isotones were ordered in the sense that the small $\log_{10}T_c$ against cluster emission corresponds to relatively high stability of the produced daughter with respect to the larger value of $\log_{10}T_c$. We applied this measure of detecting magic numbers and relative stability to the minima that appeared in the whole range of N and Z considered in the present paper. We predicted the neutron magic or semimagic numbers $N = 126$,148, 152, 160, 162, 172, 178, and 184 and the proton magic numbers $Z = 82$, 98, 102, 106, 108, 114, and 116. These magic nucleon numbers agree with the magic numbers deduced by minimizing the total energy of a nucleus or from self-consistent calculations and other different methods. Moreover, we predicted the neutron magic or semimagic numbers $N = 154$, 176, 180, 182, and 200.

[1] A. Sandulescu, D. N. Poenaru, and W. Greiner, Sovt. J. Part. Nucl. **11**, 528 (1980).
[2] H. J. Rose and G. A. Jones, Nature (London) **307**, 245 (1984).
[3] D. V. Aleksandrov, A. F. Belyatski, Y. A. Glukhov, E. Y. Nikolski, B. G. Novatski, A. A. Ogloblin, and D. N. Stepanov, JETP Lett. **40**, 909 (1984).
[4] S. Gales, E. Hourani, M. Hussonnois, J. P. Schapira, L. Stab, and M. Vergnes, Phys. Rev. Lett. **53**, 759 (1984).
[5] P. B. Price, J. D. Stevenson, S. W. Barwick, and H. L. Ravn, Phys. Rev. Lett. **54**, 297 (1985).
[6] D. Weselka, P. Hille, and A. Chalupka, Phys. Rev. C **41**, 778 (1990).
[7] R. Bonetti *et al.*, Nucl. Phys. A **562**, 32 (1993).
[8] M. Paul, I. Ahmad, and W. Kutschera, Phys. Rev. C **34**, 1980 (1986).
[9] K. J. Moody, E. K. Hulet, S. Wang, P. B. Price, and S. W. Barwick, Phys. Rev. C **36**, 2710 (1987).
[10] S. Wang, D. Snowden-Ifft, P. B. Price, K. J. Moody, and E. K. Hulet, Phys. Rev. C **39**, 1647 (1989).
[11] R. Bonetti, C. Chiesa, A. Guglielmetti, C. Migliorino, A. Cesana, M. Terrani, and P. B. Price, Phys. Rev. C **44**, 888 (1991).
[12] G. Audi, F. G. Kondev, M. Wang, B. Pfeiffer, X. Sun, J. Blachot, and M. MacCormick, Chin. Phys. C **36**, 1157 (2012), and references therein.
[13] S. G. Kadmenskii, S. D. Kurgalin, and Y. M. Chuvil'skii, Phys. Part. Nucl. **38**, 699 (2007).
[14] W. M. Seif, M. Shalaby, and M. F. Alrakshy, Phys. Rev. C **84**, 064608 (2011).
[15] S. Peltonen, D. S. Delion, and J. Suhonen, Phys. Rev. C **75**, 054301 (2007).
[16] W. M. Seif, Phys. Rev. C **74**, 034302 (2006).
[17] Y. Qian, Z. Ren and D. Ni, Nucl. Phys. A **866**, 1 (2011).
[18] M. Ismail and A. Adel, Phys. Rev. C **89**, 034617 (2014).
[19] W. M. Seif, M. M. Botros, and A. I. Refaie, Phys. Rev. C **92**, 044302 (2015)
[20] C. Xu, Z. Ren, G. Röpke, P. Schuck, Y. Funaki, H. Horiuchi, A. Tohsaki, T. Yamada, and B. Zhou, Phys. Rev. C **93**, 011306(R) (2016).
[21] M. Bhattacharya, S. Roy, and G. Gangopadhyaya, Phys. Lett. B **665**, 182 (2008).
[22] M. Ismail, A. Y. Ellithi, M. M. Botros, and A. Adel, Phys. Rev. C **81**, 024602 (2010).
[23] W. M. Seif, J. Phys. G: Nucl. Part. Phys. **40**, 105102 (2013).

[24] Y. Ren and Z. Ren, Phys. Rev. C **85**, 044608 (2012).
[25] H. F. Zhang and G. Royer, Phys. Rev. C **77**, 054318 (2008).
[26] Y. Qian, Z. Ren, and D. Ni, J. Phys. G: Nucl. Part. Phys. **38**, 015102 (2011).
[27] W. M. Seif, Phys. Rev. C **91**, 014322 (2015).
[28] S. Hofmann, J. Phys. G: Nucl. Part. Phys. **42**, 114001 (2015).
[29] S. Hofmann, *On Beyond Uranium: Journey to the End of the Periodic Table* (Taylor & Francis, London, 2003).
[30] S. S. Malik and R. K. Gupta, Phys. Rev. C **39**, 1992 (1989).
[31] B. Buck and A. C. Merchant, Phys. Rev. C **39**, 2097 (1989).
[32] R. G. Lovas, R. J. Liotta, A. Insolia, K. Varga, and D. S. Delion, Phys. Rep. **294**, 265 (1998).
[33] S. N. Kuklin, G. G. Adamian, and N. V. Antonenko, Phys. Rev. C **71**, 014301 (2005).
[34] H. F. Zhang, J. M. Dong, G. Royer, W. Zuo, and J. Q. Li, Phys. Rev. C **80**, 037307 (2009).
[35] C. Xu and Z. Ren, Phys. Rev. C **74**, 014304 (2006).
[36] M. Ismail and W. M. Seif, Phys. Rev. C **81**, 034607 (2010).
[37] C. Xu and Z. Ren, Phys. Rev. C **73**, 041301(R) (2006).
[38] G. F. Bertsch, J. Borysowicz, H. Mcmanus, and W. G. Love, Nucl. Phys. A **284**, 399 (1977).
[39] G. R. Satchler and W. G. Love, Phys. Rep. **55**, 183 (1979).
[40] M. Ismail, W. M. Seif, and H. El-Gebaly, Phys. Lett. B **563**, 53 (2003).
[41] K. W. Ford and J. G. Wills, Phys. Rev. **185**, 1429 (1969).
[42] J. D. Walecka, *Theoretical Nuclear Physics and Subnuclear Physics* (Oxford University, Oxford, 1995), p. 11.
[43] M. J. Rhoades-Brown, V. E. Oberacker, M. Seiwert, and W. Greiner, Z. Phys. A: Condens. Matter **310**, 287 (1983).
[44] M. Ismail, W. M. Seif, A. Y. Ellithi, and F. Salah, J. Phys. G: Nucl. Part. Phys. **35**, 075101 (2008).
[45] B. Buck, A. C. Merchant, and S. M. Perez, Phys. Rev. C **45**, 2247 (1992).
[46] N. G. Kelkar and H. M. Castañeda, Phys. Rev. C **76**, 064605 (2007).
[47] M. Ismail, A. Y. Ellithi, M. M. Botros, and A. Abdurrahman, Phys. Rev. C **86**, 044317 (2012).
[48] B. Buck, J. C. Johnston, A. C. Merchant, and S. M. Perez, Phys. Rev. C **53**, 2841 (1996).
[49] B. Buck, A. C. Merchant, S. M. Perez, and P. Tripe, J. Phys. G: Nucl. Part. Phys. **20**, 351 (1994).
[50] D. Ni and Z. Ren, Phys. Rev. C **82**, 024311 (2010).
[51] A. Soylu, Y. Sert, O. Bayrak, and I. Boztosun, Eur. Phys. J. A **48**, 128 (2012).
[52] W. M. Seif, M. Ismail, A. I. Refaie, and L. H. Amer, J. Phys. G: Nucl. Part. Phys. **43**, 075101 (2016).
[53] S. A. Gurvitz and G. Kälbermann, Phys. Rev. Lett. **59**, 262 (1987).
[54] M. Wang, G. Audi, A. H. Wapstra, F. G. Kondev, M. MacCormick, X. Xu, and B. Pfeiffer, Chin. Phys. C **36**, 1603 (2012).
[55] P. Möller, J. R. Nix, W. D. Myers, and W. J. Swiatecki, At. Data Nucl. Data Tables **59**, 185 (1995).
[56] D. Ni, Z. Ren, T. Dong, and C. Xu, Phys. Rev. C **78**, 044310 (2008).
[57] M. Ismail and A. Adel, Phys. Rev. C **90**, 064624 (2014).
[58] M. Ismail, A. Y. Ellithi, A. Adel, and H. Anwer, J. Phys. G: Nucl. Part. Phys. **43**, 015101 (2016), and references therein.
[59] A. A. Saldanha, A. R. Farhan, and M.M. Sharma, J. Phys. G: Nucl. Part. Phys. **36**, 115103 (2009).
[60] G. A. Lalazissis, M. M. Sharma, P. Ring, and Y. K. Gambhir, Nucl. Phys. A **608**, 202 (1996).
[61] M. Ismail and A. Adel, Int. J. Mod. Phys. E **21**, 1250062 (2012).
[62] D. N. Poenaru, R. A. Gherghescu, and W. Greiner, Phys. Rev. C **85**, 034615 (2012).
[63] K. P. Santhosh and R. K. Biju, Pramana **72**, 689 (2009).
[64] S. Ćwiok, S. Hofmann, and W. Nazarewicz, Nucl. Phys. A **573**, 356 (1994).
[65] S. Liran, A. Marinov, and N. Zeldes, Hyperfine Interact. **132**, 421 (2001).
[66] W. Zhang, J. Meng, S. Q. Zhang, L. S. Gengand, and H. Toki, Nucl. Phys. A **753**, 106 (2005).
[67] J. H. Hamilton, S. Hofmann, and Y. T. Oganessian, J. Phys.: Conf. Ser. **580**, 012019 (2015).
[68] D. N. Poenaru and W. Greiner, *Heavy Elements and Related New Phenomena* (World Scientific, Singapore, 1999), Vol. II.
[69] P. Möller and J. R. Nix, J. Phys. G: Nucl. Part. Phys. **20**, 1681 (1994).
[70] X. J. Bao, H. F. Zhang, J. M. Dong, J. Q. Li, and H. F. Zhang, Phys. Rev. C **89**, 067301 (2014).
[71] P. T. Greenlees, R.-D. Herzberg, S. Ketelhut, P. A. Butler, P. Chowdhury, T. Grahn, C. Gray-Jones, G. D. Jones, P. Jones, R. Julin, S. Juutinen, T.-L. Khoo, M. Leino, S. Moon, M. Nyman, J. Pakarinen, P. Rahkila, D. Rostron, J. Sarén, C. Scholey, J. Sorri, S. K. Tandel, J. Uusitalo, and M. Venhart, Phys. Rev. C **78**, 021303 (2008).
[72] R. V. Jolos, in *EXON-2012-Proceedings of the International Symposium, Vladivostok, Russia, 2012*, edited by Y. E. Penionzhkevich and Y. G. Sobolev (World Scientific, Singapore, 2013), p. 147.
[73] T. Sil, S. K. Patra, B. K. Sharma, M. Centelles, and X. Viñas, Phys. Rev. C **69**, 044315 (2004).
[74] W. M. Seif and H. Mansour, Int. J. Mod. Phys. E **24**, 1550083 (2015).
[75] D. Ni and Z. Ren, Phys. Rev. C **93**, 054318 (2016).
[76] M. Ismail and A. Adel, Phys. Rev. C **88**, 054604 (2013).
[77] B. Sahu and S. Bhoi, Phys. Rev. C **93**, 044301 (2016).